Detecting galaxy clusters through optimal filtering: weak lensing, SZ and X-rays

Dr. Matteo Maturi
ITA, Zentrum für Astronomie, Universität Heidelberg,
Albert Überle Str. 2, 69120 Heidelberg, Germany

January 12, 2008

Abstract

We aim at detecting galaxy clusters with a multiwavelength approach base on a linear matched filter capable of maximizing the signal to noise ratio of weak gravitational lensing, X-rays and SZ cluster detections. The method also provides unbiased estimates of cluster properties, such as DM and baryonic content. We use ray-tracing through a large cosmological hydrodynamic simulation to construct realizations of the three different observables between redshifts zero and two. We apply the filters mentioned above to detect peaks in the weak-lensing, X-rays and SZ signals and compare them with the true population of dark matter halos present in the simulation.

1 The numerical simulations

We used a hydrodynamical, N-body simulation, carried out with the code GADGET-2 (Springel, 2005) to produce mock observation of typical weak lensing surveys ($n_{gal} = 30/arcmin^2$, $\sigma_\gamma = 0.3$, two realizations with the background sourced at $z_s = 1$ and $z_s = 2$), the X-rays observatories XMM Newton (EPIC) and Chandra (ACIS I) with exposures time of $30ks$ and $100ks$, and the next generation millimetric observatory ACT (the three channels: 145, 225 and 265 GHz).

1.1 Weak gravitational lensing simulation

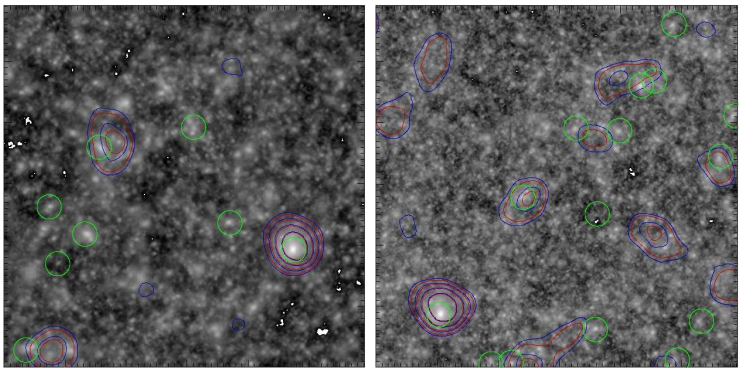

Figure 1: Example maps of the effective convergence for sources at redshift $z_s = 1$ (left panel) and $z_s = 2$ (right panel) for a region of simulated sky. The positions of the halos contained in the field-of-view having mass $M > 7 \times 10^{13} h^{-1} M_\odot$ are identified by circles.

1.2 Sunjaev Zel'dovich effect simulation

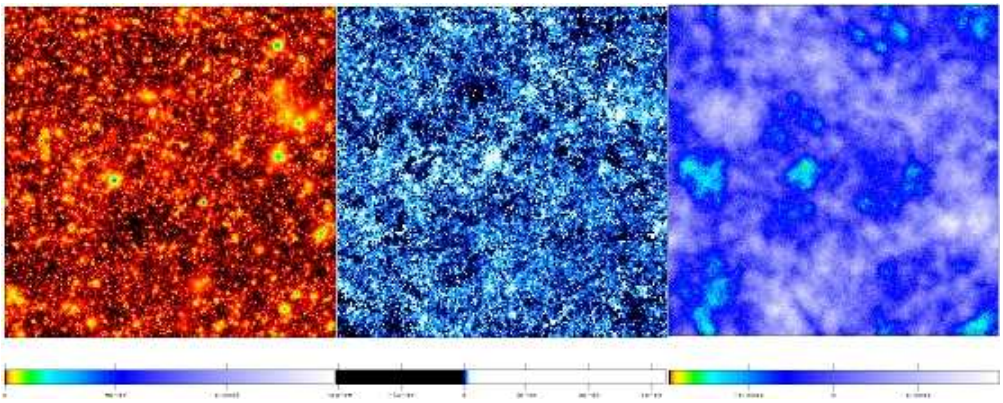

Figure 2: Example maps of the SZ effect including cosmic structures up to redshift $z = 1$. On the left, we show a simulated map of the tSZ effect, on the central panel we show a simulated map of the kSZ effect and on the right we show the same field as observed with ACT in the 145 GHz channel, including the kSZ effect, the CMB and the instrumental noise.

1.3 X-rays simulations

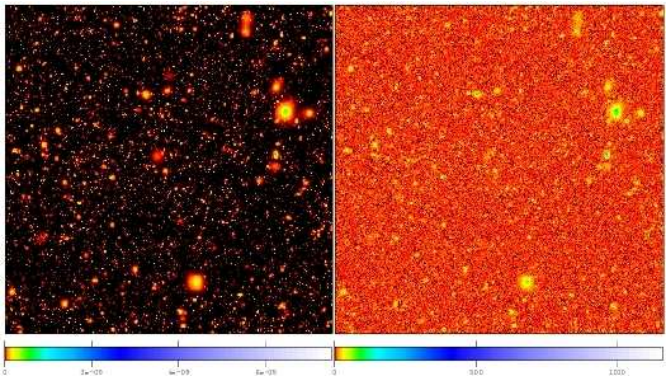

Figure 3: Left panel: example map of the X-ray flux in the soft band for the same structures shown in Fig. 2. Right panel: example simulated observation with XMM-*Newton*, assuming an exposure time of 30 ks.

2 The optimal matched filter

This filter allows to combine information from different bands. The data obtained at a given frequency ν are written as

$$D_\nu(\boldsymbol{\theta}) = S_\nu(\boldsymbol{\theta}) + N_\nu(\boldsymbol{\theta}) \text{ with } S_\nu(\boldsymbol{\theta}) = A f_\nu \tau_\nu(\boldsymbol{\theta}) \,, \tag{1}$$

where $S_\nu(\boldsymbol{\theta})$ and $N_\nu(\boldsymbol{\theta})$ are the signal, the noise component at the band ν, A is the (band independent) amplitude, f_ν is the frequency dependence of the amplitude and $\tau_\nu(\boldsymbol{\theta})$ is the spatial profile normalized to unity. We assume that the background noise has zero mean in each band and that its statistical properties are fully characterized by the correlation function $C_{\nu_1\nu_2}$

To measure the signal amplitude A, we simply convolve the data D with a filter kernel Ψ_ν so that the final estimate is given by

$$A_{\rm est} = \sum_{\nu=1}^{M} A_{{\rm est},\nu}(\boldsymbol{\theta}) \ . \tag{2}$$

We define the filter Ψ such that it is optimal, i.e. the variance estimate σ_A is minimal, and such that it returns an unbiased estimate $b \equiv \langle A_{est} - A \rangle = 0$. The filter which satisfies these conditions is the one which minimizes the Lagrangian $L = \sigma^2 + \alpha b$

$$\mathbf{\Psi = \alpha C^{-1} F} \ , \tag{3}$$

where $\mathbf{C}^{-1}$ is the inverse of the matrix $\mathbf{C}$ and α is a Lagrangian multiplier given by

$$\alpha^{-1} = \mathbf{F}^{\rm T}\mathbf{C}^{-1}\mathbf{F} \ . \tag{4}$$

Eq. 3 shows that the matched filter depends on the noise, taking advantage of its correlation between all bands. In the particular case $P_{\nu_1\nu_2} = P_{\nu_1}\delta(\nu_1 - \nu_2)$, i.e. in the case of non correlated noise, the matrix $\mathbf{C}$, and therefore its inverse, is diagonal with each element associated to the noise power-spectrum.

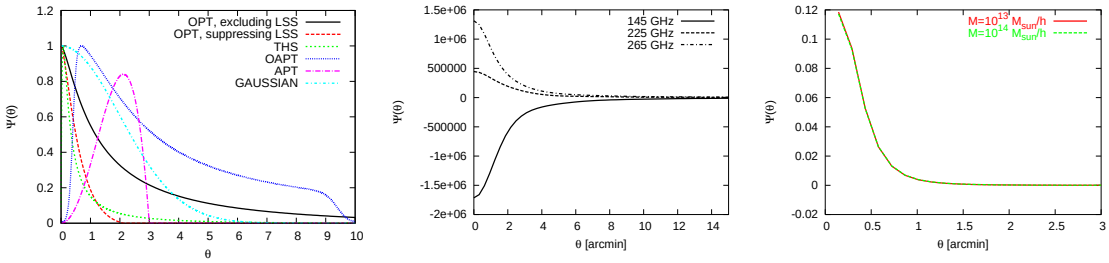

Figure 4: This figure shows how the filter depends on the signal and its noise properties. Left panel: weak lensing optimal filter (OPT) compared with the aperture mass (APT and OAPT) and a gaussian filter tuned through numerical simulations (Gaussian). Central panel: the three filters used simultaneously to analyze the 145 GHz, 225 GHz and 265 GHz channels of the SZ observations. Right panel: The filter used in the X-ray observations.

3 Detections number

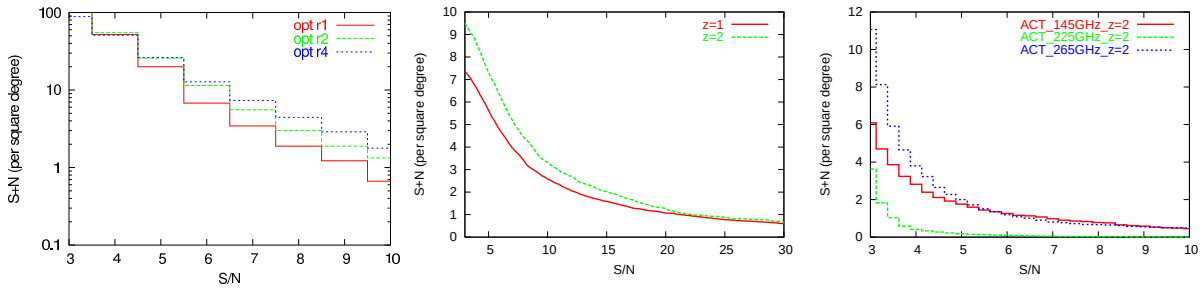

Figure 5: Detection number with respect to their signal-to-noise ratio for weak lensing (left), X-rays (middle) and SZ effect (right) respectively. Comparable number of detections for weak lensing and X-rays observations.

4 Contamination fraction

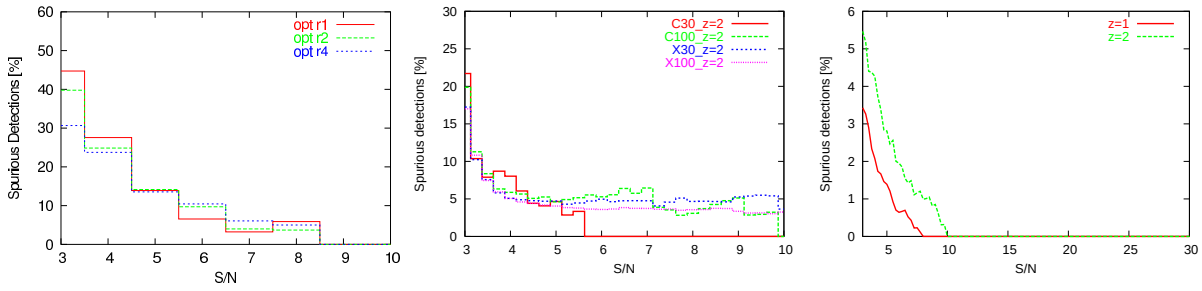

Figure 6: Number of spurious detections with respect to their signal-to-noise ratio for weak lensing (left), X-rays (middle) and SZ effect (right) respectively. The weak lensing contamination is larger but comparable to the X-rays one. The SZ sample has the lowest contamination level.

5 Completeness

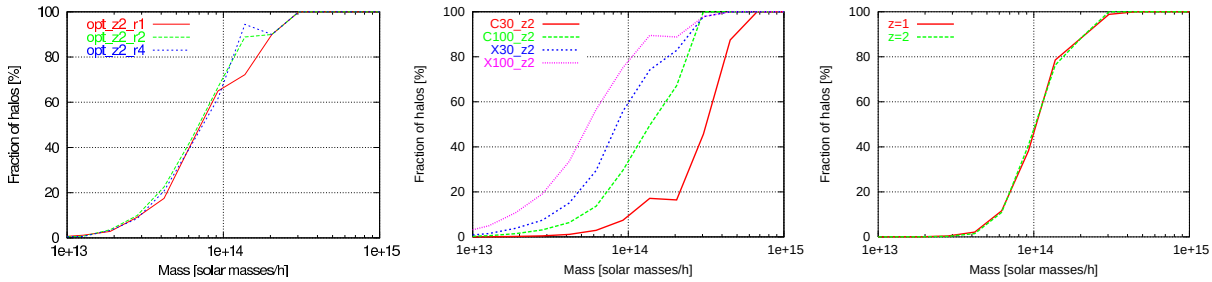

Figure 7: Fraction of detected haloes with respect to their mass for weak lensing (left), X-rays (middle) and SZ effect (right) respectively. The results obtained with all three observables are comparable.

6 Sensitivity

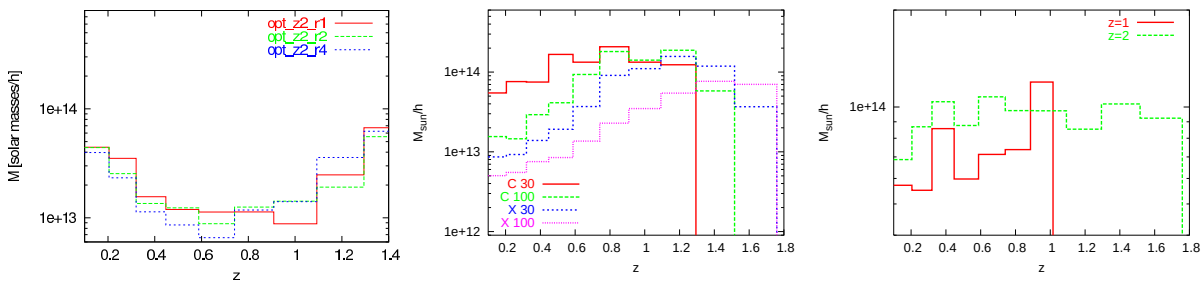

Figure 8: Minimum detected haloes mass with respect to their redshift for weak lensing (left), X-rays (middle) and SZ effect (right) respectively. Smaller masses can be probed with weak lensing.

7 SZ X-rays detection correlation

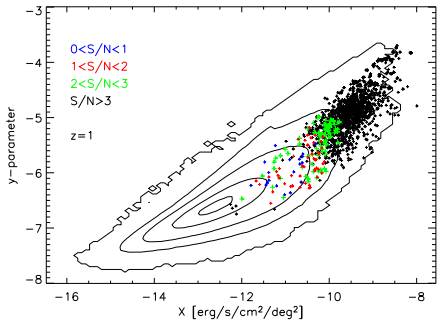

Figure 9: Correlation between the estimated Compton parameter (y-axed) and X-ray flux (x-axis). We show the common detections with corresponding to different signal-to-noise ratios (blue for $0 < S/N < 1$, red for $1 < S/N < 2$, yellow for $2 < S/N < 3$ and black for $S/N > 3$). The iso-contours shows the expected correlation which perfectly match with the estimates.

8 Conclusions and future work

- We aim at detecting galaxy clusters using all available observables together (linear filter):
  - Weak lensing
  - X-rays
  - Sunyaev Zel'dovich effect
  - Galaxy counting (still to come)
- This is optimal to search for clusters as they are expected to be, but it should also point at peculiar objects (X-ray silent clusters, etc.).
- Next step 1: include galaxy surveys (with photometric redshifts).
- Next step 2: combine all observables in a multi-band filter to obtain a single S/N map out of all observables.

References

Borgani, S., Murante, G., Springel, V., et al. 2004, MNRAS, 348, 1078

Borgani, S., Rosati, P., Tozzi, P., & Norman, C. 1999, ApJ, 517, 40

Dietrich, J., Erben, T., Lamer, Schneider, P., Schwope, Hartlap, & Maturi, M., L. 2007, ApJ, 470, 821

Maturi, M., Meneghetti, M., Bartelmann, M., Dolag, K., & Moscardini, L. 2005, A&A, 442, 851

Maturi, M., Schirmer, M., Bartelmann, M., Meneghetti, M., & Moscardini, L. 2007, A&A, 662, 473

Pace, F., Maturi, M., Meneghetti, M., et al. 2007, A&A, 471, 731

Springel, V. 2005, MNRAS, 364, 1105